Saudi Journal of Biological Sciences 28 (2021) 7190–7201

Contents lists available at ScienceDirect

Saudi Journal of Biological Sciences

journal homepage: www.sciencedirect.com

Original article

Amelioration of indole acetic acid-induced cytotoxicity in mice using zinc nanoparticles biosynthesized with *Ochradenus arabicus* leaf extract

Khalid Mashai Alanazi [a], Ahmed Ali Al-kawmani [a], Mohammad Abul Farah [a,**], Waleed Ali Hailan [a], Ali Alsalme [b], Nabil Al-Zaqri [b], M. Ajmal Ali [c,*], Abobakr Mahmood Almansob [c]

[a] Department of Zoology, College of Science, King Saud University, P.O. Box 2455, Riyadh 11451, Saudi Arabia
[b] Department of Chemistry, College of Science, King Saud University, P.O. Box 2455, Riyadh 11451, Saudi Arabia
[c] Department of Botany & Microbiology, College of Science, King Saud University, P.O. Box 2455, Riyadh 11451, Saudi Arabia

ARTICLE INFO

Article history:
Received 26 June 2021
Revised 2 August 2021
Accepted 3 August 2021
Available online 11 August 2021

Keyword:
Apoptosis
ROS generation
DNA damage
Genotoxicity
Indole acetic acid
Zinc nanoparticle

ABSTRACT

The diversity of natural phytochemicals represents an unlimited source for discovery and development of new drugs. *Ochradenus arabicus*, (family: Resedaceae) a notable medicinal plant displays a high content of flavonoid glycosides. This study investigates a possible preventative role of zinc nanoparticles biosynthesized by *O. arabicus* leaf extracts (OAZnO NPs) in limiting genotoxicity and cytotoxicity caused by indole acetic acid (IAA) in laboratory mice. ZnO NPs were synthesized using *O. arabicus* leaf extracts and characterized with UV–visible spectroscopy, scanning electron microscopy (SEM) and X-Ray diffraction (XRD). The mice were randomly distributed into the following six groups: control, OAZnO NPs treated (10 mg/kg BW), IAA treated (50 mg/kg BW); simultaneous treatment, pre-treatment, and post-treatment. Reactive oxygen species (ROS), DNA damage, chromosome aberration, and apoptosis were analyzed as toxicity endpoints. IAA exposure significantly induced production of ROS, DNA damage, apoptosis, chromosome aberrations, and micronuclei. Pre-, post-, and simultaneous treatment with OAZnO NPs ameliorated the damage caused by IAA exposure. Exposure to OAZnO NPs alone caused no toxicity for any endpoint based on comparison to controls. This study demonstrated that IAA-induced cytotoxic damage in mice could be ameliorated by treatment with OAZnO NPs. These findings require additional verification in mechanistic and *in vitro* studies.

1. Introduction

Indole acetic acid (IAA) is a naturally occurring plant growth phytohormone. Previous studies on the toxic effects of IAA often focused on genotoxicity and genomic changes in mammalian cells (Furukawa et al. 2005; Jeong et al. 2010). The ability of IAA to induce intracellular generation of ROS may cause DNA damage, increase apoptosis, and ultimately stimulate carcinogenesis due to activation of p38 mitogen-activated protein kinases. IAA induces caspase-9 and caspase-8, products of polymerase cleavage, and caspase-3 activation (Jeong et al. 2010). Further, treating rats with IAA during the early stages of development of the cerebral cortex caused decreased motor activity in embryos, decreased brain size with microcephaly, genotoxicity, and apoptosis (Patten et al. 2013).

In recent years, the use of traditional plant-derived medicines has gained attention, and many studies have confirmed their efficacy for treatment of a variety of diseases in humans (Aleebrahim-Dehkordy et al. 2017). Such actions reflect the presence of important phytochemicals, such as flavonoids, terpenoids, phenolics, and alkaloids (Tungmunnithum et al. 2018). Plant-based products have been used in many areas, including medicine, nutrition, flavoring, cosmetics, and beverages (Yuan et al. 2016). Further, plant-derived products, such as grassy teas, extracts, cosmetics, and tinctures, are widely used for preparing traditional medicines. Certain phytochemicals in extracts of medicinal plants act as scavengers of reactive oxygen species (ROS) by donating hydrogen atoms to peroxy roots, singlet oxygen, hydroxyl radicals, and superoxide anions. Phytochemicals also act as chelators of metal ions that can induce lipid peroxidation (Li et al. 2016).

* Corresponding author.
** Corresponding author.
E-mail addresses: mfarah@ksu.edu.sa (M.A. Farah), alimohammad@ksu.edu.sa (M. Ajmal Ali).
Peer review under responsibility of King Saud University.

Production and hosting by Elsevier

https://doi.org/10.1016/j.sjbs.2021.08.015
1319-562X/

Ochradenus (Resedaceae) is a genus of plants comprising eight species common in the arid deserts of North Africa and South-West Asia. The center of diversity is the Arabian Peninsula (Al-kawmani et al. 2020). *Ochradenus arabicus* is considered a valuable medicinal species in arid regions (Khan et al. 2012). Currently, plants with medicinal properties are used in the preparation of nanoparticles with silver, zinc, iron, gold, and copper. These nanoparticles can be used to treat various diseases. Their pharmacological activity reflects biocompatibility between biological components of plants and chemical makeup of nanoparticles (Santhoshkumar et al. 2017). Zinc oxide nanoparticles (ZnO NPs) were reported to have toxicological hazards *in vivo* and *in vitro*. Antibacterial, antioxidant, anticancer, and immunomodulatory effects of ZnO NPs have been reported in various studies (Huang et al. 2010, Sharma et al. 2012). However, bioengineered ZnO NPs contains bioavailability and biocompatibility that makes them very promising tools in biomedical applications with therapeutic benefits (Elshama et al. 2018).

Previous studies show that indole acetic acid increases ROS generation, inducing severe cytotoxicity via oxidative stress on lipid membranes and nucleic acids (Folkes and Wardman 2001; de Melo et al. 2004). IAA enhances apoptosis, necrosis (loss of membrane integrity), chromatin condensation, and DNA fragmentation (Wardman 2002). The present study performed biosynthesis of zinc oxide nanoparticles using *O. arabicus* leaf extracts (OAZnO NPs), and investigated their protection against oxidative stress, genotoxicity, and cytotoxicity (apoptosis) induced by IAA in an experimental animal model (mice).

2. Materials and methods

2.1. Plant material and preparation of the extract

Fresh *O. arabicus* leaves were randomly collected (November 2019) from wild habitat around Riyadh, Saudi Arabia (24°43′10″N, 46°36′55″E). The plant species was documented by plant taxonomists in the Centre of Biodiversity and Plant Taxonomy, Department of Botany, King Saud University. The collected leaves (50 gm) were rinsed thoroughly with MilliQ water, then cut into small sections. The leaves from sterile stems were air-dried in the dark at 20 ± 5 °C for 12 days. Dried plant leaves were made powder using an electric blender. Finally, an aqueous extract was prepared as described by Santhoshkumar et al. (2017), with slight modifications.

2.2. Biosynthesis and characterization of ZnO NPs

ZnO NPs were biosynthesized as described by Chaudhuri and Malodia (2017). Briefly, 2.195 g zinc acetate dihydrate (Lot # MKBQ7110v obtained from Sigma-Aldrich) mixed with 35 mL Milli-Q water was dissolved in 10 mL of *O. arabicus* leaf extract. The reaction mixture was stirred for 6 h. Two molar NaOH (obtained from Sigma-Aldrich) was added to the solution, and incubated overnight at 60 °C with magnetic stirring (Chaudhuri and Malodia 2017). The mixture was then centrifuged at 10,000 rpm for 10 min and the precipitate was washed twice with distilled water. The precipitate was dried at 60 °C in an incubator. The fine powder was used for characterization using a scanning electron microscope (SEM), Energy dispersive X -ray spectoroscopy (EDX), X-ray diffraction (XRD), and ultraviolet–visible spectroscopy (UV–Vis spectroscopy) (Chaudhuri and Malodia 2017).

2.3. Selection of doses

A short term acute toxicity test was conducted in mice to determine LD_{50} doses of OAZnO NPs and IAA (Sigma chemical company, USA). The LD_{50} value of OAZnO NPs and IAA were 150, and 100 mg/kg BW, respectively. Treatments were administered using oral gavage. OAZnO NPs and IAA doses were 10 and 50 mg/kg of BW, respectively, both notably below LD50 values (Hassan et al. 2019).

2.4. Animals and treatment

Male mice (SWR/J) between 10 and 12 weeks old, weighing (25–28) g, were selected randomly. Mice were purchased from the Experimental Animal Care Center, Department of Pharmacy, King Saud University, Riyadh, KSA. Animals were housed in cages and maintained in an environmentally controlled room with a temperature of 22 °C, a relative humidity of 45%, and a dark/light cycle of 12 h. They were provided with food (commercial mouse pellets) and water *ad libitum* throughout the experiment. All protocols were followed, and experiments conducted in strict compliance with the ethical principles and guidelines of the Animal Ethics Committee, King Saud University, Riyadh, KSA (Ethics References No. SE-19–127).

The experiment consisted of six groups (n = 6): pre-, simultaneous- and post-treatment groups, an OAZnO NPs treatment group, and positive (IAA) and negative (distilled water) control groups. After 22 days of treatment, mice were euthanized by cervical dislocation. Bone marrow, liver tissues, and peripheral blood were collected for analysis. The following treatments were administered to mice of different groups via gavage for 22 days.

Control group (distilled water 0.5 mL/kg BW), OAZnO NPs group (10 mg/kg BW), IAA (50 mg/kg BW); simultaneous treatment group OAZnO NPs (10 mg/kg BW) and IAA (50 mg/kg BW), pre-treatment group OAZnO NPs (10 mg/kg BW) for 18 days followed by IAA (50 mg/kg BW) until the 22nd day (four days), and post-treatment group IAA (50 mg/kg BW) on the first four days and then OAZnO NPs (10 mg/kg BW) for the next 18 days. Fig. 1 is showing the experimental plan for the treatment of mice in six different groups through a scheme.

2.5. ROS assay

A commercial kit (Image-iT™ LIVE Green ROS Detection Kit, Molecular Probes, USA) was used to determine ROS levels in bone marrow cells. Mice were euthanized by cervical dislocation, and bone marrow was removed (Bagri and Jain 2019). Bone marrow cells were mixed well with NaCl (0.9%), and 100 μL of cell suspension was stained with the working solution (25 μM) of carboxy-H_2DCFDA stain provided in the kit. Liver cells were incubated at 38 °C in a water bath for 35 min. Quantitative analysis was performed as described by Liu et al. (2018). Similarly, qualitative analysis of ROS generation by fluorescence microscopic imaging was performed by transferring 10–20 μL of cells onto a glass slide. The images were captured using appropriate filter settings with a microscope (Olympus BX41, Japan) fitted with a fluorescence attachment and CCD camera.

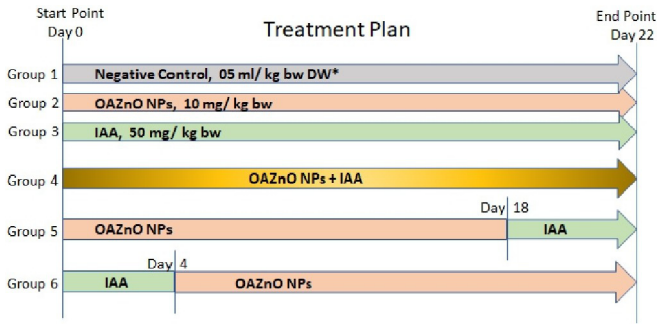

Fig. 1. Schematic representation of experimental plan for the treatment of mice in different six groups. DW*, distilled water.

2.6. Comet assay

Bone marrow cells were used for the comet assay. Cell suspension was embedded in layers of agarose gel on slides and allowed to unwind for 20 min in electrophoresis buffer (pH > 13), followed by electrophoresis for 25 min. Slides were stained with 15 μg/mL of ethidium bromide and analyzed under a fluorescence microscope using an appropriate filter. Alkaline comet tests for DNA damage were performed as previously described (Zhang et al. 2018a). Lengths of the comet tails were divided into five classes (0, 1, 2, 3, and 4), and total DNA damage points were calculated as described by Ali et al. (2019).

2.7. TUNEL assay

Liver tissue paraffin sections obtained from treated and control mice were used for the detection of DNA fragmentation using a TUNEL assay kit (FITC-labeled, Genescript, USA). Briefly, tissue samples were processed following the manufacturer's protocol. 50 μL of TUNEL Reaction Mixture was added to each sample. A coverslip was placed over the sample and incubated for 50–60 min at 37–38 °C under moist conditions in the dark. The slides were washed three times with a 70% saline solution for 4–5 min and changes were observed under a fluorescence microscope with an excitation wavelength of 450–500 nm and an emission wavelength of 515–565 nm.

2.8. Annexin V-FITC apoptosis assay by flow cytometry

After treatment, liver cell suspensions were prepared in PBS using a cell strainer with 100 mm pore size. Samples of liver cell suspensions were washed and centrifuged. After the final wash, cells were resuspended in 100 μL of 1× binding buffer. The cell suspension were stained using a commercial kit containing Annexin-V-FITC and propidium iodide (BD Biosciences, San Jose, CA, USA) for the differentiation of early and late apoptotic and necrotic cells using flow cytometry (BD FACS Calibur).

2.9. Micronucleus (MN) test

MN tests on peripheral blood were performed as described by Hayashi et al. (1988) and Hayashi (2016), with some modifications. Peripheral blood was collected by cutting tail tips. Blood smears

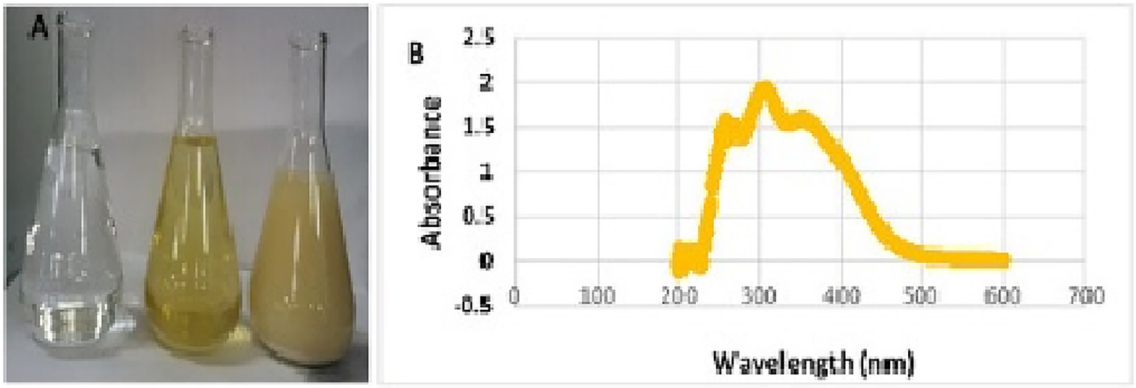

Fig. 2. (A) The color of reaction mixtures changed from yellow to white (B) UV–vis spectrum for OAZnO NPs showing absorption at wavelength at 320 nm.

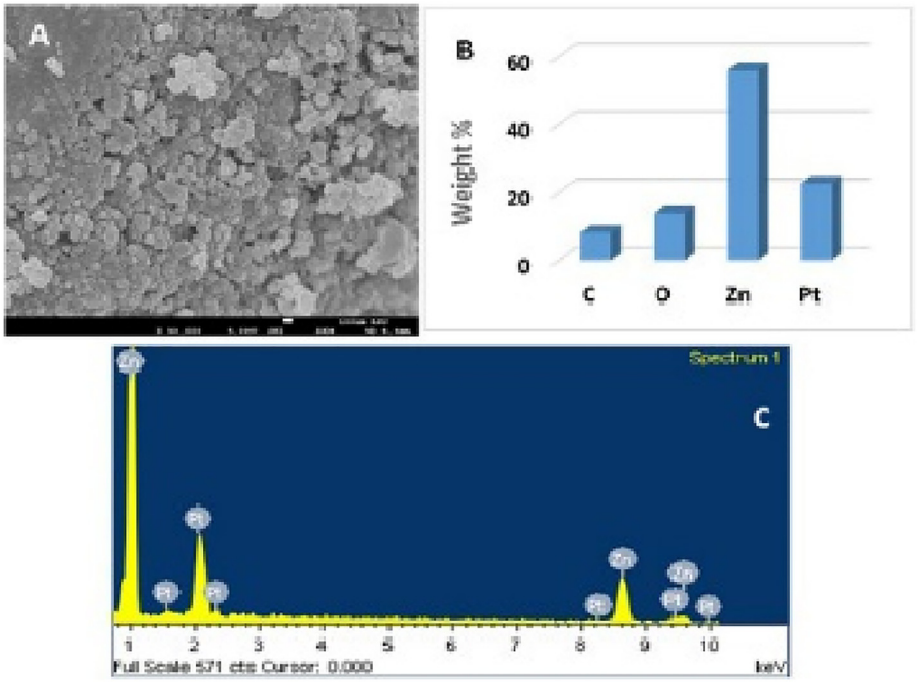

Fig. 3. (A) Scanning electron microphotograph of OAZnO NPs at 30,000× magnifications, (B) and (C) elementals weight percent from the EDX pattern.

Table 1
Genotoxic effect of all treatments on bone marrow cells in Mice using the comet assay.

Group	Total Count	Cells per damage class					Total DNA damage	%Total DNA damage	TDS
		0	1	2	3	4			
Control	500	465	30	5	0	0	35	7	40
OAZnO NPs	500	450	30	15	3	2	50	10	77
AAI	500	360	70	51	10	9	140	28	238**
Per-treatment	500	411	51	31	4	3	89	17.8	137*
Post-treatment	500	410	54	30	3	3	90	18	135*
Simu-treatment	500	445	30	20	3	2	55	11	87

TDS: total damage score.
* $p < 0.05$.
** $p < 0.01$.

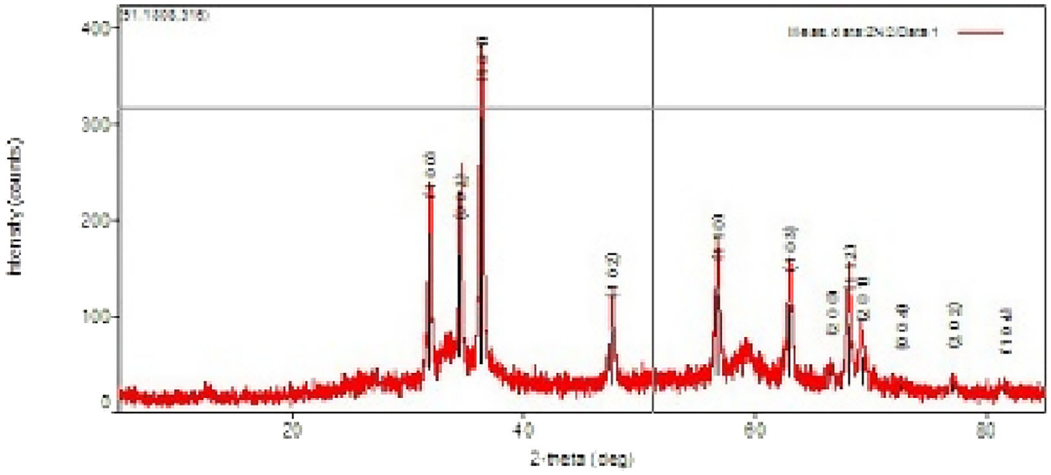

Fig. 4. X-ray diffraction (XRD) pattern of OAZnO NPs.

were prepared on clean microscope slides, air-dried, fixed in absolute methanol for 10 min, and stained with acridine orange (125 μg/mL in pH 6.8 phosphate buffer) just before evaluation. Slides were coded and observed using a fluorescence microscope (Olympus, BX41, Tokyo, Japan) at 40× magnification with appropriate filter settings. Micronucleated cells were identified by scoring 2000 polychromatic erythrocytes (PCEs) per animal to identify clastogenic and aneugenic potential of the test compound. Possible cytotoxic effects were assessed using the PCE/NCE (normal/chromatic erythrocyte) ratio in 200 erythrocytes/animals (Gollapudi and McFadden 1995).

2.10. Chromosomal aberrations

After treatments, mice were injected with 0.05% colchicine (0.1–0.12 mL/kg BW). After 1.30–2 h., mice were euthanized by cervical dislocation. Chromosome aberrations were tested in bone marrow cells as previously reported (Abou-Tarboush and Abdel-Samad 2010), and accurately described by Prasad et al. (2009). Cells were stained with 10% Giemsa and analyzed following the methods of Al-Anazi (2015). Briefly, structural changes (breaks, gaps, acentric fragments, etc.) and numerical aberrations were analyzed under an Olympus® BX41 microscope using a 100× oil immersion objective lens. Mitotic index was also calculated by observing 2000 cells from each animal (n = 4) (Al-Anazi, 2015).

2.11. Statistical analysis

All experiments were performed in triplicate to assure data reproducibility. Data are presented as mean ± SE. One -way ANOVA was used to determine the significance of the data. *P-values* < 0.05 were considered statistically significant. Statistical analyses were performed with SPSS software (SPSS Inc., Chicago, IL, USA).

Table 2
Frequency of micronucleus induced treatments in the peripheral blood of mice exposed to indicate doses 22 day duration.

Groups	No. all cells	No. NCE	No. PCE	No. MN	PCE / NCE mean ± SE	MN/PCE mean ± SE
Control	8000	7843	157	5	2.00 ± 0.22[a]	3.19 ± 0.29[a]
OAZnO NPs	8000	7881	119	7	1.51 ± 0.23[a]	5.9 ± 0.23[a]
IAA	8000	7937	63	21	0.79 ± 0.25[b]	33.59 ± 0.22[b]
pre-treatment	8000	7930	70	13	0.88 ± 0.21[c]	18.56 ± 0.20[c]
post-treatment	8000	7926	74	14	0.93 ± 0.21[c]	18.95 ± 0.26[c]
simu-treatment	8000	7883	117	15	1.49 ± 0.22[a]	12.71 ± 0.23[c]

Columns with different superscripts are significantly affects a-e (P < 0.001).
Values were represented as means ± SE.
2000 PCE were analyzed for each animal (n = 4).

Table 3
Genotoxic effect of all treatments on bone marrow cells in mice using the chromosome aberration.

Groups	No. of Metaphase	Numerical aberrations			Mean (%) ± SD	Structural aberrations						Mean (%) ± SD
		Hypo	Hyper	Poly		B	R	F	CAd	D	Pulv	
Controls	200	3	3	1	2.6 ± 0.75	1	1	5	6	0	2	5.96 ± 0.77
OAZnO NPs	200	21	6	5	3.65 ± 1.54	4	4	7	6	5	10	10.42 ± 2.2*
IAA	200	13	7	9	7.15 ± 1.88*	3	2	4	7	3	5	22.06 ± 2.2*
Per-treatment	200	9	2	5	4.34 ± 1.22*	3	4	6	8	4	2	18.3 ± 3.12*
Post-treatment	200	16	11	4	4.97 ± 2.1*	4	3	6	12	5	9	18.98 ± 2.7*
Simu-treatment	200	3	4	2	3.74 ± 0.88	1	0	4	5	0	2	15 ± 0.65

* Significant ($p < 0.05$) Hypo- Hypoploidy; Hyper- Hyperploidy; Poly- Polyploidy; B- Break; R- Ring; F- Fragment; Cad- Centromeric Adhesion; D- Deletion; Pulv- Pulverization.

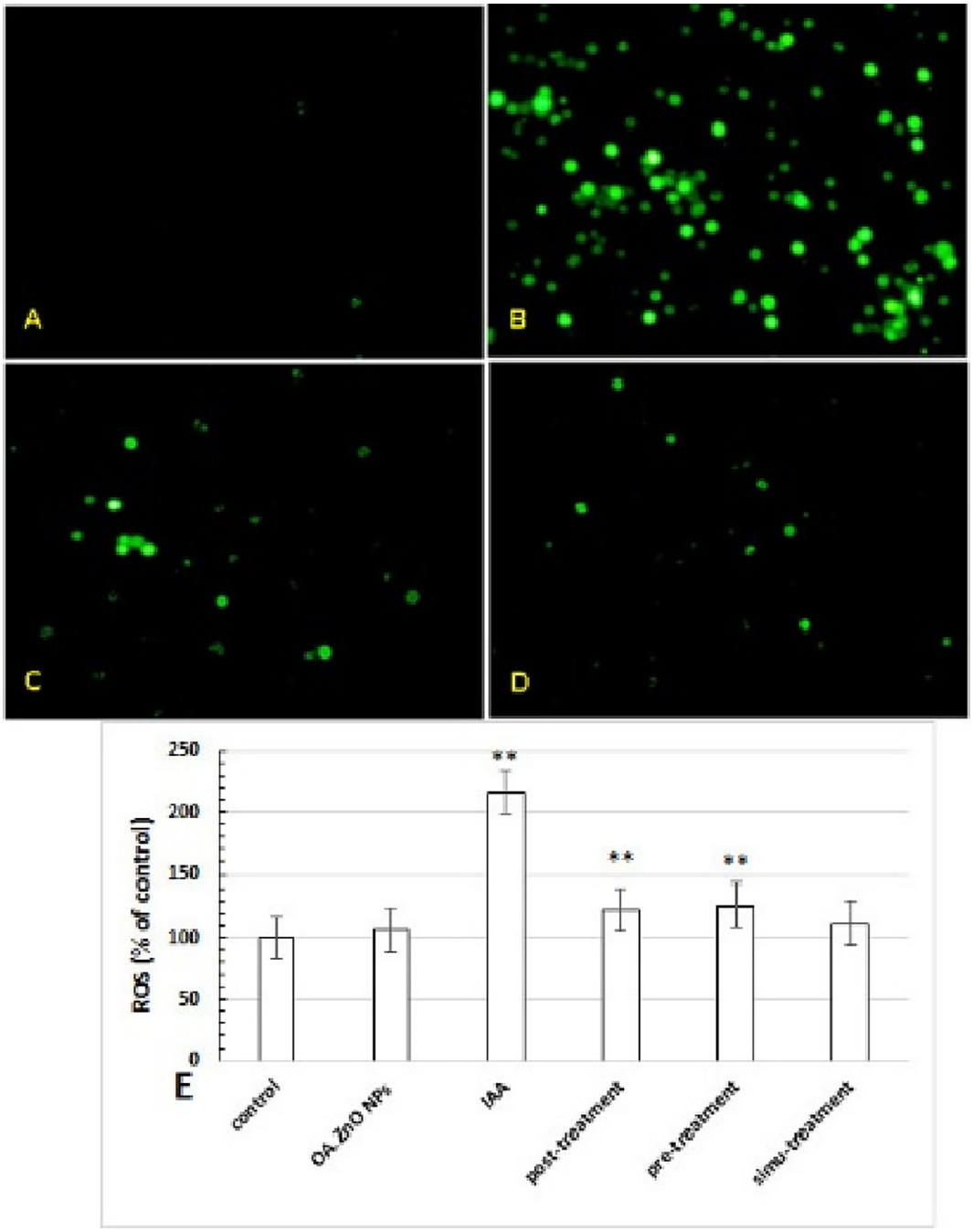

Fig. 5. Representative images of bone marrow cells of mice stained with DCFDA showing generation of reactive oxygen species (ROS). (A) Control, (B) IAA (50 mg/kg) BW, (C) pretreatment, and (D) simultaneous treatment. Magnification; 20×. (E) Effect of treatments on the ROS generation of liver cells in mice. An increase or decrease in ROS level is shown as a percentage relative to the control, set at 100%. **Significant ($p < 0.01$).

3. Results

3.1. Biosynthesis and characterization of ZnONPs

UV–visible spectral analysis was used to investigate reducing capacity of *O. arabicus* aqueous extract used for the biosynthesis of ZnO NPs. The color of the reaction mixture was initially yellowish, then changed to off-white Fig. 2A. This change in color was observed at 372 nm. UV–visible spectra of synthesized microwave-assisted ZnO NPs are shown in Fig. 2B.

Scanning electron microscopic images show variations in the size and shape of NPs (Fig. 3A). Two-dimensional geometry of the NPs was identified as circular, elliptical, and slightly hexagonal or irregular. Average size of the NPs was 55 nm. The EDX pattern identifies zinc with the highest elemental weight percent (55.94%) (Fig. 3B). Oxygen, carbon, and Sulphur made up 13.60, 7.76, and 22.71%, respectively (Fig. 3C).

X-ray diffraction (XRD) was used to measure average nanoparticle sizes. The diffraction pattern biosynthesized ZnO NPs is provided in Fig. 4. Bragg reflection was set to be prominent at (2θ), where values were observed at 33°, 35°, 38°, 44°, 59°, 62°, 65°, 65°, 71°, 74°, 78°, and 83° with intensities of 100, 002, 101, 102, 110, 103, 200, 112, 201, 004, 202, and 102, respectively. The full width-at-half-maximum value of 45° was used to account for NP

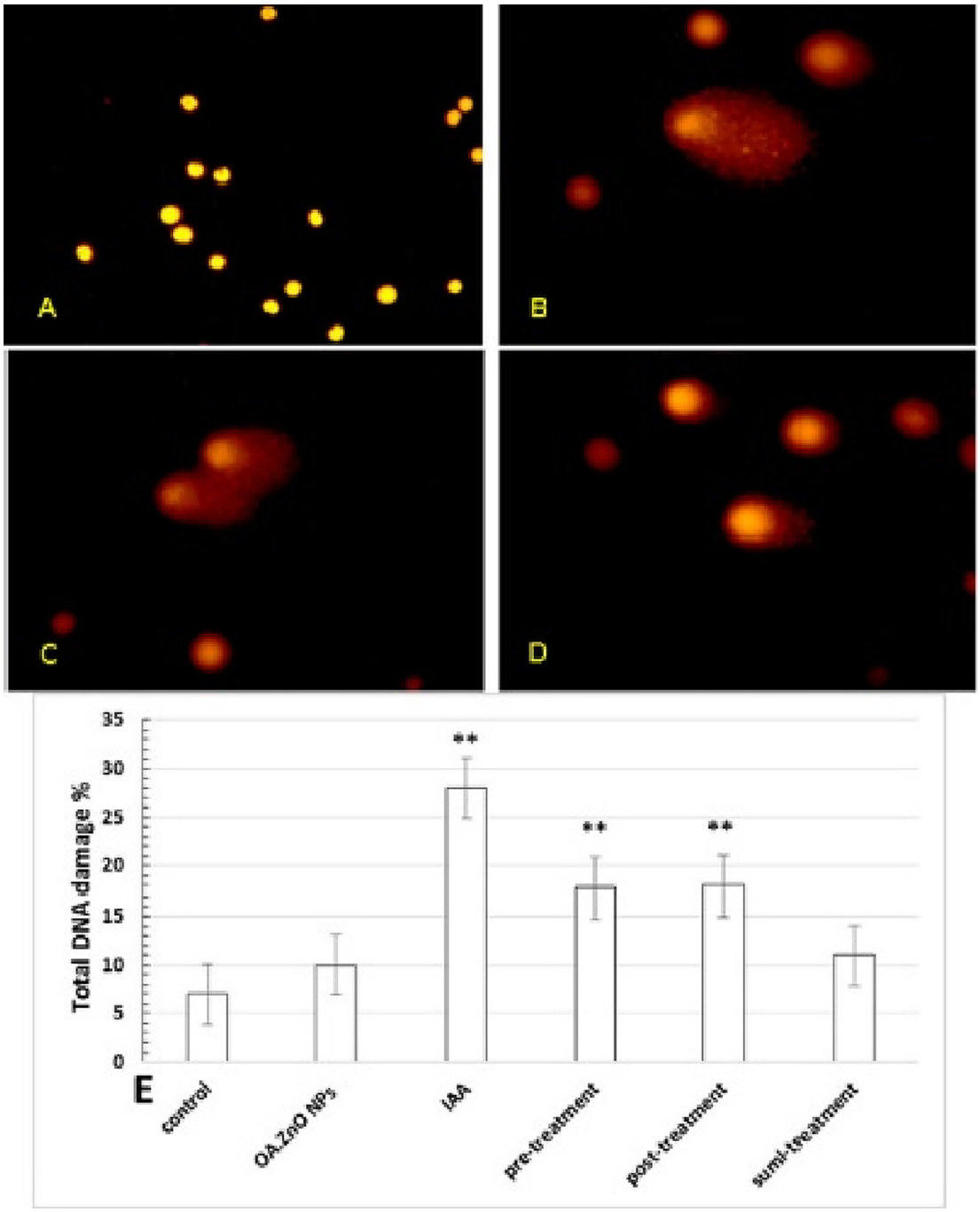

Fig. 6. Representative images of bone marrow cells of mice stained with ethidium bromide showing DNA damage analyzed by comet assay. (A) Control, (B) IAA, (C) post-treatment, and (D) simultaneous treatment. Magnification; 40×. (E) The effect of different treatments on the % total DNA damage. An increase or decrease of total DNA damage is shown as a percentage relative to control. **Significant ($p < 0.01$).

size. The average NP size was 55 nm. This value is consistent with the results obtained using SEM.

3.2. ROS assay

After treatments, a substantial increase in ROS generation in the bone marrow cells was reflected by the intensity of green fluorescence compared with the control mice, where low levels of fluorescence were detected (Fig. 5A-D). Fluorescence in the OAZnO NPs and simultaneous treatment groups was similar to the control group. Fluorescence levels in pre- and post-treatment groups were less intense compared to the IAA group. Quantitative estimates of fluorescence showed that ROS in the IAA treatment group increased significantly ($p < 0.01$) compared to other groups. A maximum ROS level of 115% was recorded after 22 days of treatment with IAA (50 mg/kg of BW), while ROS levels were 6.56% after treatment with OAZnO NPs (10 mg/kg of BW). Finally, the pre- and post-treatment, as well as the simultaneous treatment group, showed increases in ROS levels of 26.02%, 22.45%, and 11.59%, respectively, compared with the control group (Fig. 5E). These ROS levels were significantly lower than ROS levels in the IAA group.

3.3. Comet assay

Representative images of comets obtained after treatments are provided in Fig. 6 A-D, and quantitative results from this assay were shown in Table 1 and Fig. 6E. Total damage scores in all treatment groups were 238, 137, 135, 77, 87, and 40, for IAA, OAZnO NPs, pre-, post- and simultaneous treatments, respectively. Significant differences ($p < 0.01$) in percentages of DNA fragmentation between IAA and pre- and post-treatment groups but not simultaneous treatment and OAZnO NPs groups were noted when compared with the control group.

3.4. Cytotoxicity analysis (apoptosis) by TUNEL assay

Representative images obtained from the TUNEL assay of apoptotic effects of IAA, pre- and post-treatment, OAZnO NPs, and simultaneous treatment are provided in Fig. 7A-D. An increase in apoptosis in cells (green spots) was observed in pre- and post-treatment groups compared with the control, OAZnO NPs, and simultaneous treatment groups. The apoptotic cells stained by TUNEL when treated with IAA remarkably increased, indicating high numbers of hepatocytes as a result of IAA intoxication.

3.5. Annexin-V apoptosis assay using flow cytometry

Apoptosis was measured using flow cytometry. In controls, only 1.56% of cells were in the late apoptosis stage (Annexin V + ve/PI + ve), and necrosis was not observed (Fig. 8A-F). OAZnO NPs and simultaneous treatments displayed no increase in early and late apoptosis or necrosis. The highest early and late apoptosis and necrosis events were observed in IAA exposed mice (10.14%, 7.63%, and 5.53%, respectively), percentages were lower in pre- (8.32%, 7.2%, and 2.39%, respectively) and post-treatment (8.15%, 8.53%, and 4.04%, respectively) groups relative to the control group (Fig. 8G).

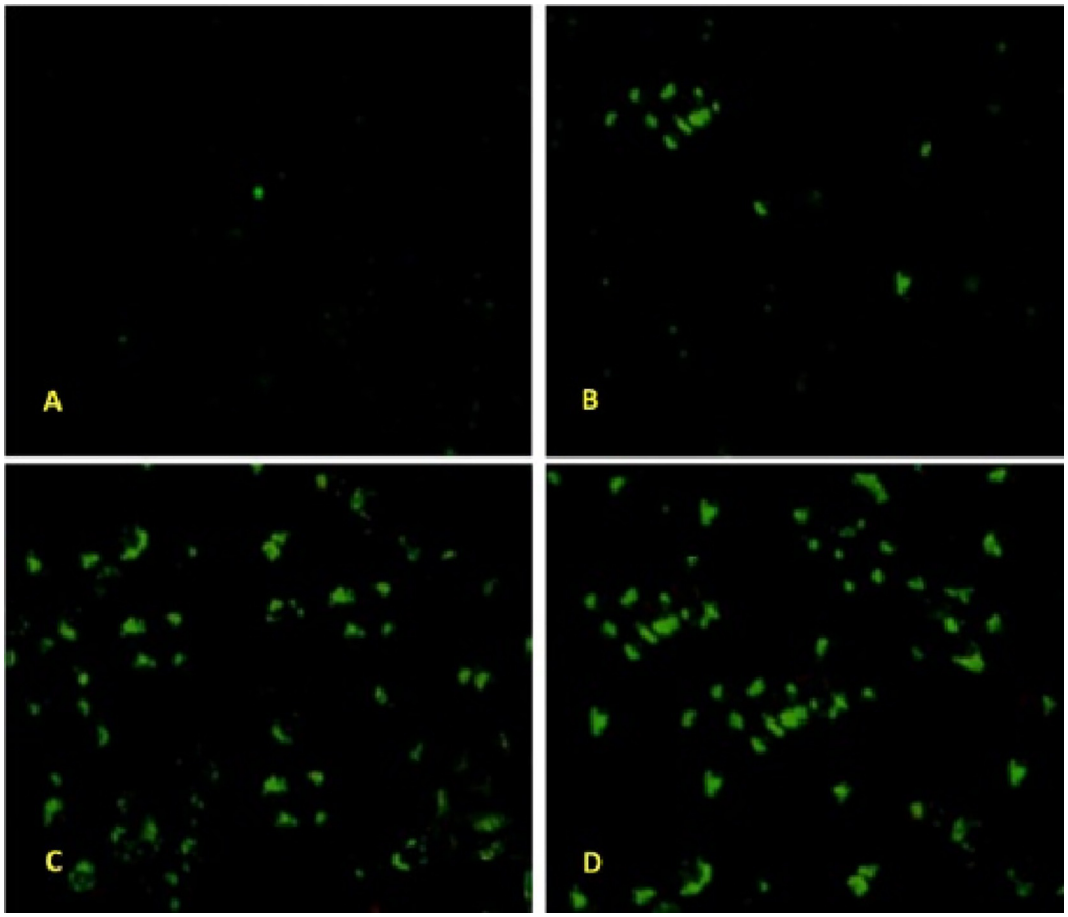

Fig. 7. Representative images of the liver cells of mice showing the effects of different treatments on TUNEL apoptosis assay results (FITC-Labeled Kit). (A) Control, (B) simultaneous treatment, (C) pretreatment, and (D) IAA. Magnification; 20×.

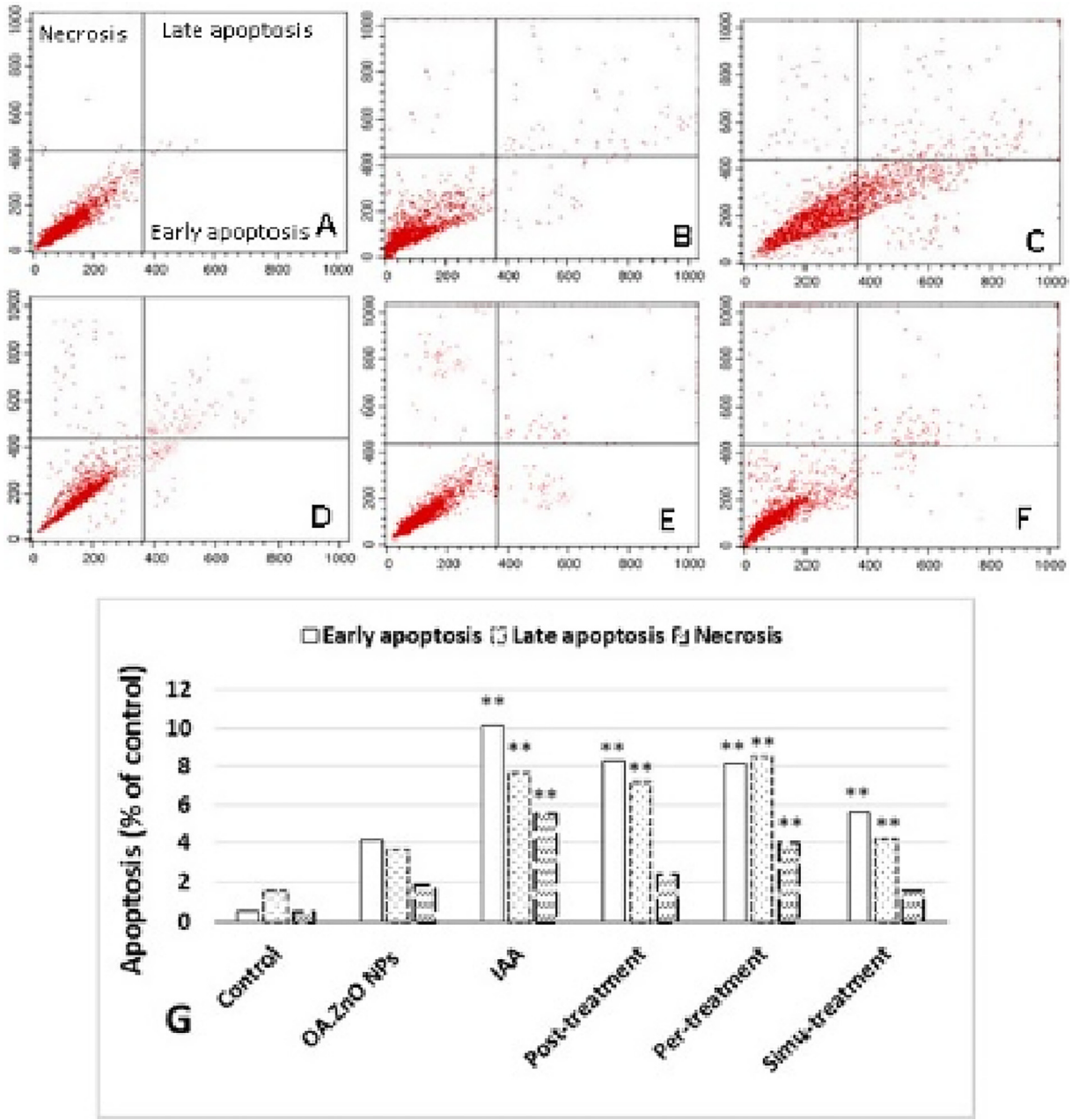

Fig. 8. Apoptosis detection by annexin V-FITC/PI staining of liver cells analyzed by flow cytometry showing (A) Control, (B) OAZnO NPs, (C) IAA alone, (D) post-treatment (E) pretreatment, and (F) simultaneous treatment. (G) The effect of different treatments on the early and late apoptosis and necrosis of liver cells in mice. The values are expressed as mean ± Standard Error (SE), (*Significant, p < 0.05).

3.6. Micronucleus assay

Representative images of MN obtained after treatments of mice were provided in Fig. 9A-D. Genotoxic effects are shown in Table 2 and Fig. 9E. The incidence of MN in the pre- and post-treatment groups increased, and MN frequency increased significantly ($p < 0.01$) in IAA-treated compared with control group mice. The frequency of MN recorded after IAA was (33.59 ± 0.22). A frequency of 12.71 ± 0.23 was observed for simultaneous treatment. IAA-treated mice showed a significant ($p < 0.01$) decrease in numbers (PCE/NCE) compared to other treatment groups. In summary, treatments (pre- and post-treatment and simultaneous treatment) significantly reduced the MN levels compared to that in the IAA group.

3.7. Chromosomal aberrations

Chromosome aberrations in mice after IAA, pre- and post-treatment, OAZnO NPs, and simultaneous treatment showed a significant increase compared with the controls (Table 3). The representative images for normal and aberrant metaphases are shown in Fig. 10A-D. Mitotic indices of bone marrow cells were shown in Fig. 10E. Mitotic index significantly decreased ($p < 0.05$) in treatment groups compared to the control groups.

4. Discussion

ZnO NPs were successfully synthesized in the present study. A similar result was reported for synthesis of ZnO NPs with an inter-

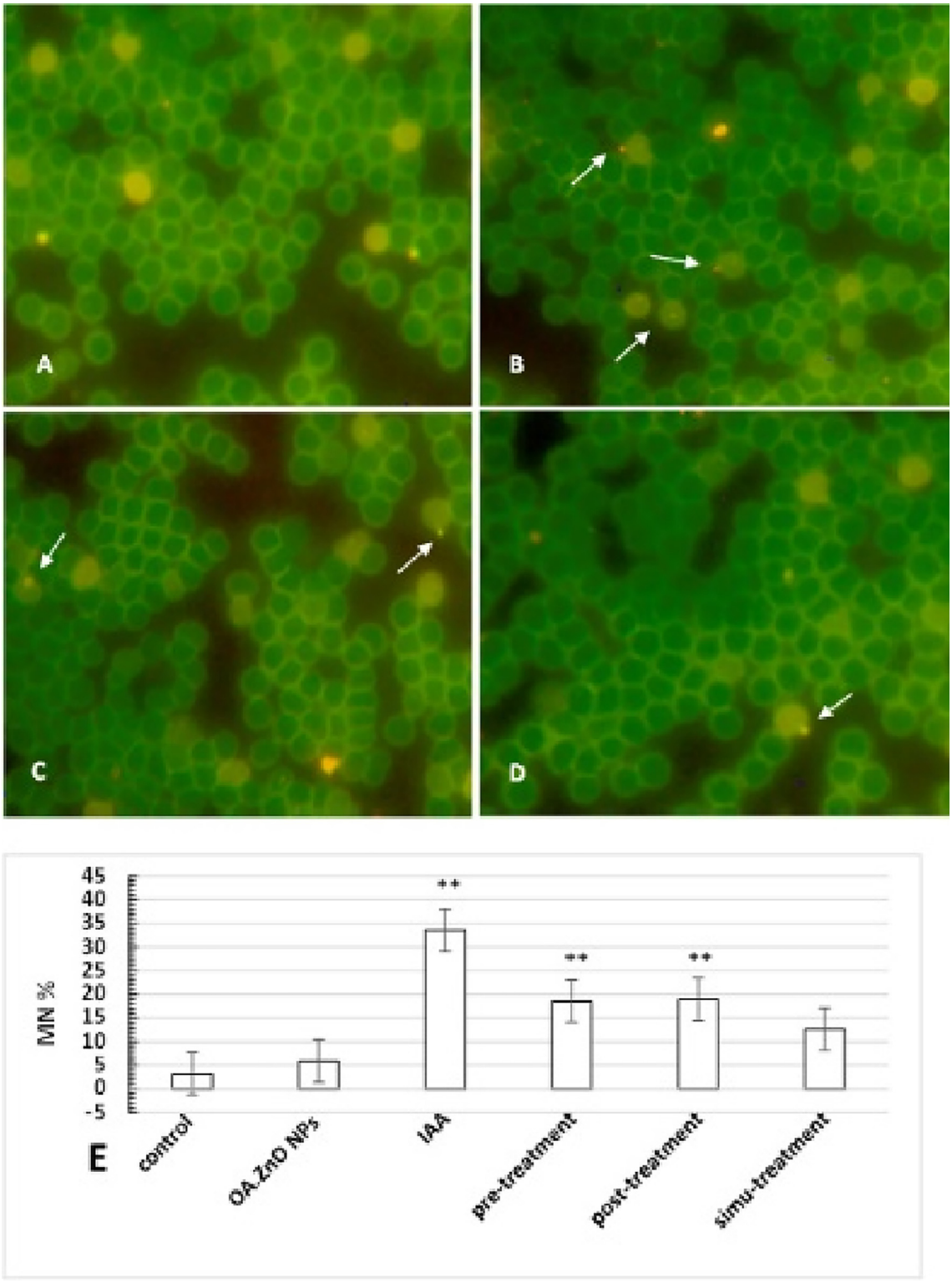

Fig. 9. Representative images of peripheral blood cells of mice showing the effects of different treatments on MN. (A) Control, (B) simultaneous treatment, (C) pretreatment, and (D) IAA alone. Magnification 40×. (E) The effect of different treatments on MN of bone marrow cells of mice. An increase or decrease of MN is shown as a percentage relative to control. **Significant ($p < 0.01$).

esting absorbance peak of approximately 372 nm (Al-Shabib et al. 2016, Khatami et al. 2018, Hassan et al. 2019). ZnO NPs synthesized from leaf extracts of *O. arabicus* showed an absorption maximum in the range of 357–378 nm due to surface plasmon resonance (Liu et al. 2016, Chaudhuri and Malodia 2017, Hassan et al. 2019). SEM and EDX analyses are routinely used identification of the shape and size of nanoparticles. These parameters for nanoparticles in this study were similar to the shape and size of nanoparticles reported by Al-Shabib et al. (2018) and Hassan et al. (2019). Dried powder of AOZnO NPs was used for X-ray diffraction for an estimate of the size of the NPs. Results were almost identical to results reported by Chaudhuri and Malodia

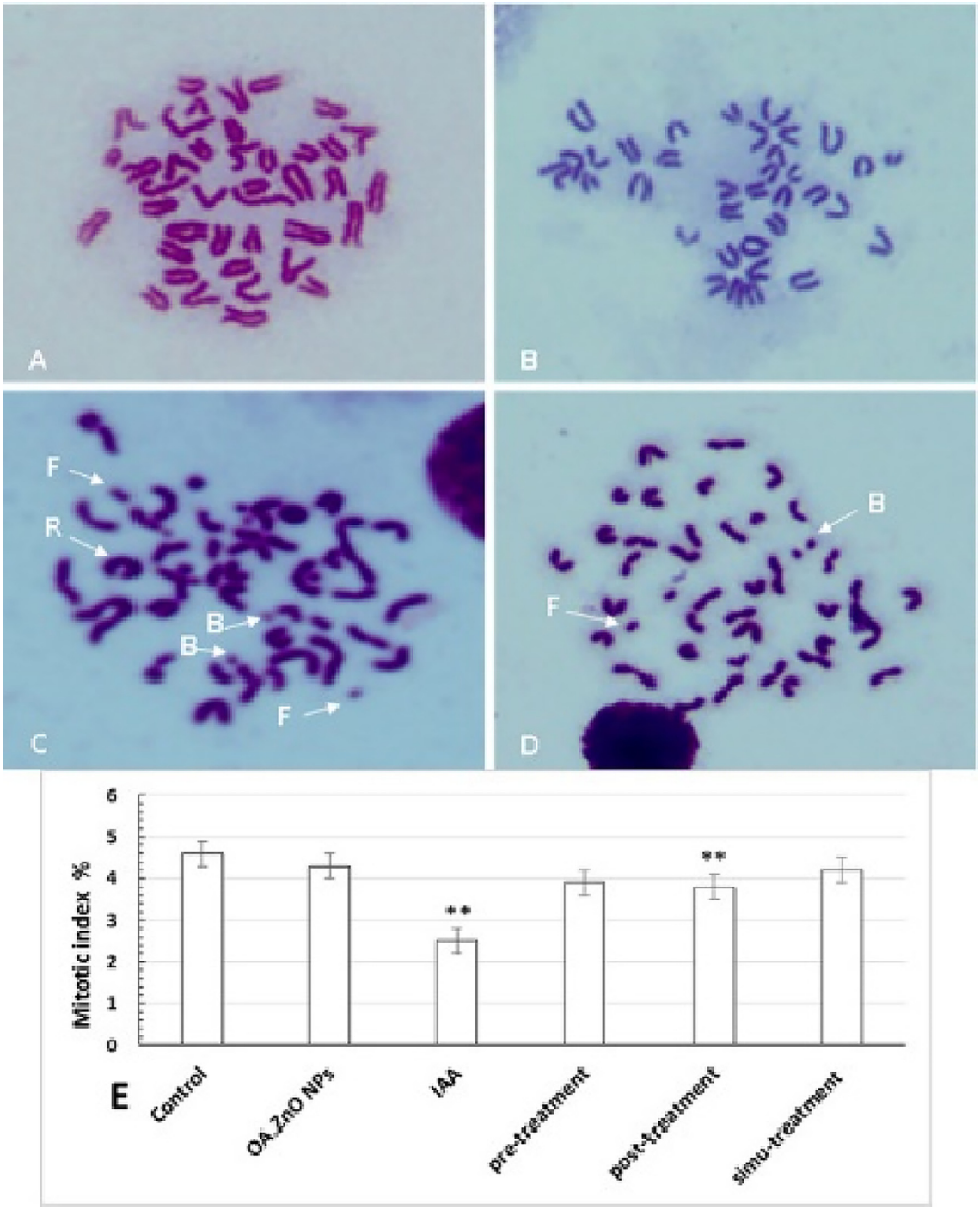

Fig. 10. Representative images of the bone marrow cells of mice stained with 10% Giemsa stain showing the effects of different treatments on chromosomal aberration. (A) Control, (B) OAZnO NPs, (C) IAA, and (D) simultaneous treatment. Magnification; 100×. (B; Break, R; Ring, F; Fragment, D; Deletion). The white arrows indicate chromosomal aberration. (E) Mitotic index for different treatments. **Significant ($p < 0.01$).

(2017) for particles synthesized with *Calotropis gigantea* extracts, with 2θ values acquired at 32.25°, 34.88°, 36.70°, 47.97°, 56.99°, 63.23°, 66.79°, 68.33°, 69.43°, and 77.39°.

ROS are produced by organisms as a normal product of metabolism. Free radicals and antioxidants are currently used to assess underlying mechanisms of chronic diseases (Lobo et al. 2010). In the present study, ROS generation was confirmed in IAA-injected mice in all treatment groups. These results were like results in previous studies (Al-Shabib et al. 2016; Hassan et al. 2019). Short-term oxidative stress may occur in tissues injured by trauma, infection, heat, hyperoxia, toxins, or excessive exercise. The generation of ROS is closely related to oxidative stress, and may cause toxicity by damaging DNA, proteins, and lipids (Schieber and Chandel 2014). The generation of intracellular ROS leads to significant and continuous changes in cell signal transduction and gene expression that may lead to cell death via apoptosis or necrosis (Bhattacharyya et al. 2014). IAA causes an increase in oxidative stress associated with loss of membrane integrity, DNA fragmentation and chromatin condensation, and apoptosis (de Melo et al. 2004). As expected, IAA stimulated the generation of ROS, DNA

damage, apoptosis, and MN and chromosome aberration compared to the control group in this study. These findings are consistent with previous studies (de Melo et al. 2004; Hassan et al. 2019). Genotoxicity of IAA was evaluated by Salopek-Sondi et al. (2010); however, mechanisms involved in apoptosis induced by IAA were not determined. Antioxidant enzymes can detect Zn2+ ions in cells, and these ions can augment the activity of primary antioxidant enzymes in pretreated cells (Cho et al. 2011). In this study, the treatment with OAZnO NPs (pre- and post-treatment and simultaneous) significantly reduced this damage. OAZnO NPs might have entered target cells and may have blocked the production of oxidizing enzymes (SOD, CAT, GR, and GPx), thereby reducing cell toxicity caused by IAA. Since natural phytochemicals present in *O. arabicus* extract acted as a stabilizing and reducing agent for the synthesis of ZnO NPs. The antioxidants, such as phenols would attached to the biosynthesized ZnO NPs, might have suppressed the expression of oxidizing enzymes and, thus, reduce generation of ROS and DNA damage. Further, OAZnO NPs appear stable in alkaline pH environments (Cho et al. 2011); however, when cellular pH decreases because of increased ROS levels caused by IAA, cells become semi-oxidized and, thus, the potential for apoptosis increases.

Apoptosis is a complex process that involves numerous energy-dependent molecular reactions (Redza-Dutordoir and Averill-Bates, 2016). IAA-induced apoptosis was confirmed as the primary mode of cytotoxicity using TUNEL and annexin V-FITC/ propidium iodide assays, which are standard methods for apoptosis analysis. A high rate of apoptosis in mice treated with IAA was observed. However, when OAZnO NPs and simultaneous treatments were administered, no increase in early and late apoptosis or necrosis occurred. *In vitro* apoptosis leads to plasma membrane permeabilization (secondary necrosis). However, this event does not occur *in vivo* because apoptotic cells are digested by macrophages or surrounding cells before plasma membranes become non-functional (Zhang et al., 2018b).

MN frequency and chromosomal aberrations are essential for measuring levels of DNA damage. Stimulation of the micronucleus formation by chromosome fragmentation can be easily distinguished kinetically or by centromere detection using molecular tests (OECD 2016). However, because most antioxidants prevent ROS production and programmed cell death, OAZnO NPs may not cause significant damage to DNA (Redza-Dutordoir and Averill-Bates, 2016).

The fundamental reason for conducting genotoxicity studies is to evaluate a compound's potential as a carcinogen, mutagen, or teratogen (OECD 2016). OAZnO NPs appear to lack genotoxicity since it fails to produce significant structural or numerical aberrations. This lack of genotoxicity, again, may be due to high amounts of antioxidants, such as phenols in *O. arabicus*. OAZnO NPs may help maintain or return ROS generation normal levels and thus ameliorated the effects of IAA.

5. Conclusion

The results of this study show increased ROS generation, DNA damage, and apoptosis after exposure to IAA. IAA also induced micronucleus formation and chromosomal aberrations, decreased mitotic index and inhibited cell proliferation. The study also demonstrates successful biosynthesis of ZnO NPs using *O. arabicus* extracts. Further, oral OAZnO NPs administration to mice mitigates IAA-induced genotoxicity and cytotoxicity. ZnO nanoparticles produced using *O. arabicus* extracts is thus a promising candidate drug that requires further verification with mechanistic and *in-vitro* studies.

Declaration of Competing Interest

The authors declare that they have no known competing financial interests or personal relationships that could have appeared to influence the work reported in this paper.

Acknowledgments

The authors would like to extend their sincere appreciation to the Researchers Supporting Project number (RSP-2021/154), King Saud University, Riyadh, Saudi Arabia.

References

Abou-Tarboush, F.M., Abdel-Samad, M.F., 2010. Cytogenetic effects of sildenafil citrate (Viagra) on SWR/J mouse bone marrow cells. Saudi J. Biol. Sci. 17, 315–319.
Al-Anazi, K.M., 2015. Cytogenetic effects of heptaplatin on SWR/J mouse bone marrow cells. Pak. J. Zool. 47, 083–1088.
Aleebrahim-Dehkordy, E., Nasri, H., Baradaran, A., Nasri, P., Tamadon, M.R., Hedaiaty, M., Beigrezaei, S., Rafieian-Kopaei, M., 2017. Medicinal plants, effective plant compounds (compositions) and their effects on stomach cancer. Int. J. Prev. Med. 8, 1–7.
Ali, A.Q., Farah, M.A., Abou-Tarboush, F.M., Al-Anazi, K.M., Ali, M.A., Lee, J., Hailan, W.A., Mahmoud, A.H., 2019. Cytogenotoxic effects of *Adenium obesum* seeds extracts on breast cancer cells. Saudi J. Biol. Sci. 26, 547–553.
Al-kawmani, A.A., Alanazi, K.M., Farah, M.A., Ali, M.A., Hailan, W.A., Al-Hemaid, F.M., 2020. Apoptosis-inducing potential of biosynthesized silver nanoparticles in breast cancer cells. J. King Saud Univ. Sci. 23 (4), 2480–2488.
Al-Shabib, N.A., Husain, F.M., Ahmed, F., Khan, R.A., Ahmad, I., Alsharaeh, E., Khan, M.S., Hussain, A., Rehman, M.T., Yusuf, M., Hassan, I., 2016. Biogenic synthesis of zinc oxide nanostructures from *Nigella sativa* seed: prospective role as food packaging material inhibiting broad-spectrum quorum sensing and biofilm. Sci. Rep. 5, 1–16.
Al-Shabib, N.A., Husain, F.M., Hassan, I., Khan, M.S., Ahmed, F., Qais, F.A., Oves, M., Rahman, M., Khan, R.A., Khan, A., Hussain, A., 2018. Biofabrication of zinc oxide nanoparticle from *Ochradenus baccatus* leaves: broad-spectrum antibiofilm activity, protein binding studies, and in vivo toxicity and stress studies. J. Nanomater. 18, 1–14.
Bagri, P., Jain, S.K., 2019. Assessment of acetamiprid-induced genotoxic effects in bone marrow cells of Swiss albino male mice. Drug Chem. Toxicol. 42, 357–363.
Bhattacharyya, A., Chattopadhyay, R., Mitra, S., Crowe, S.E., 2014. Oxidative stress: an essential factor in the pathogenesis of gastrointestinal mucosal diseases. Physiol. Rev. 94, 329–354.
Chaudhuri, S.K., Malodia, L., 2017. Biosynthesis of zinc oxide nanoparticles using leaf extract of *Calotropis gigantea*: characterization and its evaluation on tree seedling growth in nursery stage. Appl. Nanosci. 7, 501–512.
Cho, W.S., Duffin, R., Howie, S.E., Scotton, C.J., Wallace, W.A., MacNee, W., Bradley, M., Megson, I.L., Donaldson, K., 2011. Progressive severe lung injury by zinc oxide nanoparticles; the role of Zn 2+ dissolution inside lysosomes. Part. Fibre Toxicol. 8, 27.
de Melo, M.P., de Lima, T.M., Pithon-Curi, T.C., Curi, R., 2004. The mechanism of indole acetic acid cytotoxicity. Toxicol. Lett. 148, 103–111.
Elshama, S.S., Abdallah, M.E., Abdel-Karim, R.I., 2018. Zinc oxide nanoparticles: therapeutic benefits and toxicological hazards. Open Nanomed. J. 2018 (5), 16–22.
Folkes, L.K., Wardman, P., 2001. Oxidative activation of indole-3-acetic acids to cytotoxic species—a potential new role for plant auxins in cancer therapy. Biochem. Pharmacol. 61, 129–136.
Furukawa, S., Usuda, K., Abe, M., Ogawa, I., 2005. Effect of indole-3-acetic acid derivatives on neuroepithelium in rat embryos. J. Toxicol. Sci. 30, 165–174.
Gollapudi, B.B., McFadden, L.G., 1995. Sample size for the estimation of polychromatic to normochromatic erythrocyte ratio in the bone marrow micronucleus test. Mutat. Res. 347, 97–99.
Hassan, I., Husain, F.M., Khan, R.A., Ebaid, H., Al-Tamimi, J., Alhazza, I.M., Aman, S., Ibrahim, K.E., 2019. Ameliorative effect of zinc oxide nanoparticles against potassium bromate-mediated toxicity in Swiss albino rats. Environ. Sci. Pollut. Res. 26, 9966–9980.
Hayashi, M., 2016. The micronucleus test-most widely used in vivo genotoxicity test. Gene Environ. 38, 2–6.
Hayashi, M., Kishi, M., Sofuni, T., Ishidate, M., 1988. Micronucleus tests in mice on 39 food additives and eight miscellaneous chemicals. Food Cosmet. Toxicol. 26, 487–500.
Huang, C.C., Aronstam, R.S., Chen, D.R., Huang, Y.W., 2010. Oxidative stress, calcium homeostasis, and altered gene expression in human lung epithelial cells exposed to ZnO nanoparticles. Toxicol. In Vitro 24, 45–55.
Jeong, Y.M., Oh, M.H., Kim, S.Y., Li, H., Yun, H.Y., Baek, K.J., Kwon, N.S., Kim, W.Y., Kim, D.S., 2010. Indole-3-acetic acid/horseradish peroxidase induces apoptosis

in TCCSUP human urinary bladder carcinoma cells. Pharmazie. Int. J. Pharm. Sci. 65, 122–126.
Khan, S., Al-Qurainy, F., Nadeem, M., Tarroum, M., 2012. Development of genetic markers for Ochradenus arabicus (Resedaceae), an endemic medicinal plant of Saudi Arabia. Genet. Mol. Res. 11, 1300–1308.
Khatami, M., Alijani, H.Q., Heli, H., Sharifi, I., 2018. Rectangular shaped zinc oxide nanoparticles: green synthesis by Stevia and its biomedical efficiency. Ceram. Int. 44, 15596–15602.
Li, J.K., Liu, X.D., Shen, L., Zeng, W.M., Qiu, G.Z., 2016. Natural plant polyphenols for alleviating oxidative damage in man: current status and future perspectives. Trop. J. Pharm. Res. 15, 1089–1098.
Liu, J., Ma, X., Jin, S., Xue, X., Zhang, C., Wei, T., Guo, W., Liang, X.J., 2016. Zinc oxide nanoparticles as adjuvant to facilitate doxorubicin intracellular accumulation and visualize pH-responsive release for overcoming drug resistance. Mol. Pharm. 13, 1723–1730.
Liu, Y., Wen, P.H., Zhang, X.X., Dai, Y., He, Q., 2018. Breviscapine ameliorates CCl4 induced liver injury in mice through inhibiting inflammatory apoptotic response and ROS generation. Int. J. Mol. Med. 42, 755–768.
Lobo, V., Patil, A., Phatak, A., Chandra, N., 2010. Free radicals, antioxidants and functional foods: Impact on human health. Pharmacogn. Rev. 4, 118–126.
OECD, 2016. Test No. 475: Mammalian Bone Marrow Chromosomal Aberration Test, OECD Guidelines for the Testing of Chemicals, Section 4, OECD Publishing, Paris. https://doi.org/10.1787/9789264264786-en.
Patten, C.L., Blakney, A.J., Coulson, T.J., 2013. Activity, distribution and function of indole-3-acetic acid biosynthetic pathways in bacteria. Crit. Rev. Microbiol. 39, 395–415.
Prasad, S., Srivastava, S., Singh, M., Shukla, Y., 2009. Clastogenic effects of glyphosate in bone marrow cells of Swiss albino mice. J. Toxicol. 2009, 1–6.
Redza-Dutordoir, M., Averill-Bates, D.A., 2016. Activation of apoptosis signalling pathways by reactive oxygen species. BBA-Mol. Cell Res. 1863, 2977–2992.
Salopek-Sondi, B., Piljac-Žegarac, J., Magnus, V., Kopjar, N., 2010. Free radical–scavenging activity and DNA damaging potential of auxins IAA and 2-methyl-IAA evaluated in human neutrophils by the alkaline comet assay. J. Biochem. Mol. Toxicol. 24, 165–173.
Santhoshkumar, J., Kumar, S.V., Rajeshkumar, S., 2017. Synthesis of zinc oxide nanoparticles using plant leaf extract against urinary tract infection pathogen. Res.-Effic. Technol. 3, (4) 459465.
Schieber, M., Chandel, N.S., 2014. ROS function in redox signaling and oxidative stress. Curr. Biol. 24, 453–462.
Sharma, V., Singh, P., Pandey, A.K., Dhawan, A., 2012. Induction of oxidative stress, DNA damage and apoptosis in mouse liver after sub-acute oral exposure to zinc oxide nanoparticles. Mutat. Res. 745, 84–91.
Tungmunnithum, D., Thongboonyou, A., Pholboon, A., Yangsabai, A., 2018. Flavonoids and other phenolic compounds from medicinal plants for pharmaceutical and medical aspects: An overview. Medicines 5, 78–93.
Wardman, P., 2002. Indole-3-acetic acids and horseradish peroxidase: a new prodrug/enzyme combination for targeted cancer therapy. Curr. Pharm. Des. 8, 1363–1374.
Yuan, H., Ma, Q., Ye, L., Piao, G., 2016. The traditional medicine and modern medicine from natural products. Molecules 21, 552–559.
Zhang, M., Cao, G., Guo, X., Gao, Y., Li, W., Lu, D., 2018a. A comet assay for DNA damage and repair after exposure to carbon-ion beams or X-rays in Saccharomyces cerevisiae. Dose-Response 16, 1–9.
Zhang, Y., Chen, X., Gueydan, C., Han, J., 2018b. Plasma membrane changes during programmed cell deaths. Cell Res. 28 (1), 9–21.